JOURNAL OF SPACECRAFT AND ROCKETS
Vol. 30, No. 6, November–December 1993

New Semiempirical Method for Computing Nonlinear Missile Aerodynamics

F. G. Moore,* L. Devan,† and T. Hymer†
Naval Surface Warfare Center Dahlgren Division, Dahlgren, Virginia 22448

A new semiempirical method has been developed to predict normal force, pitching moment, and center of pressure on missile configurations up to angles of attack of 30-deg and 0-deg roll angle. The method is based on linear theory and slender body techniques at low angle of attack and uses wind-tunnel data to derive nonlinear angle-of-attack corrections as angle of attack increases. The new improved theories include body alone, wing alone, and body-wing and wing-body interference. Although the new theory is databased, simple analytical formulas are derived that allow general use of the techniques. Comparison with the linearized approaches used in the former Naval Surface Warfare Center Dahlgren Division aeroprediction code shows significant reductions in errors of aerodynamics above about 5- to 10-deg angle of attack. Limited comparisons to other state-of-the-art engineering codes show the new theory to be as good as or better than anything known to be available for computing planar aerodynamics up to 30-deg angle of attack.

Nomenclature

A_p = planform area of the body or wing in the crossflow plane
AR = aspect ratio of a lifting surface, b^2/A_W
A_{ref} = reference area, $\pi d_{\text{ref}}^2/4$ unless otherwise specified
A_W = wing area
b = span of lifting surface that does not include body
C_{d_c} = crossflow drag coefficient
C_M = pitching moment coefficient (moment/$\frac{1}{2}\rho_\infty V_\infty^2 A_{\text{ref}} d_{\text{ref}}$)
C_{M_α} = pitching moment coefficient derivative (positive nose up)
C_N = normal force coefficient (normal force/$\frac{1}{2}\rho_\infty V_\infty^2 A_{\text{ref}}$)
C_{N_B} = body component of normal force coefficient
C_{N_L} = linear component of normal force coefficient
$C_{N_{NL}}$ = nonlinear component of normal force coefficient
$C_{N_{T(V)}}$ = vortex lift on tail surface due to wing or canard shed vortices
C_{N_w} = normal force coefficient of wing
C_{N_α} = normal force coefficient derivative
$(C_{N_\alpha})_W$, $(C_{N_\alpha})_T$ = normal force coefficient derivative of the wing or tail
C_r = root chord of lifting surface
C_t = tip chord of lifting surface
d_{ref} = reference diameter
$K_{B(W)}$, $K_{B(T)}$ = additional interference lift factor on body due to presence of wing or tail
$K_{W(B)}$, $K_{T(B)}$ = interference lift factor on wing or tail surfaces in presence of body
$k_{B(W)}$, $k_{B(T)}$ = additional interference lift factor on body due to deflection of wings or tail surfaces
$k_{W(B)}$, $k_{T(B)}$ = interference lift factor on wing or tail due to control deflection
k_1 = constant used in nonlinear wing normal force term
M_N = Mach number normal to body, $M_\infty \sin\alpha$
M_∞ = freestream Mach number
r = radius of body at location of lifting surface
s = radius of body plus wing semispan, $r + b/2$
V_∞ = freestream velocity
X_{cp} = center of pressure measured from some given point (usually nose tip or center of gravity), caliber
X_{WA} = center of gravity of wing, dorsal, or canard planform area measured from leading edge
X_0 = distance from nose tip to point from which center of pressure is measured
α = angle of attack, deg
α_c = angle of attack where wing-body interference factor starts decreasing from its slender body theory value, deg
α_D = angle of attack where wing-body interference factor reaches a minimum, deg
β = $\sqrt{M_\infty^2 - 1}$
δ_W, δ_T = wing or tail deflection, deg, positive leading edge up
η = lift of a circular cylinder of given length-to-diameter ratio to that of a cylinder of infinite length
η_0 = value of η at $M_N = 0$
λ = taper ratio, C_t/C_r
ϕ = roll position where $\phi = 0$ deg is leeward plane

Subscripts

L = linear
NL = nonlinear

Received Sept. 25, 1992; revision received Dec. 17, 1992; accepted for publication Dec. 21, 1992; presented as Paper 93-0034 at the AIAA 31st Aerospace Sciences Meeting, Reno, NV, Jan. 11–14, 1993.

*Senior Aerodynamicist, Weapons Systems Department. Associate Fellow AIAA.
†Aerospace Engineer, Aeromechanics Branch.

Introduction

FOR the past 20 years, the Naval Surface Warfare Center Dahlgren Division (NSWCDD) has been involved in developing codes to calculate aerodynamics on tactical weapons. These codes have attempted to meet the changing needs of the tactical weapons community and to keep pace with aerodynamic requirements. A recent effort[1] was undertaken to look at where we have been, where we are, and where we need to go in the future with respect to aerodynamic codes. One of the

primary needs identified in Ref. 1 was an upgrade of the NSWCDD aeroprediction code to allow Mach numbers up to 20 (including the effects of real gases), improved lift prediction with particular emphasis on low aspect ratio lifting surfaces, and improved base drag prediction. All three of these efforts were undertaken. This paper deals with the second of these objectives: providing improved lift capability. (Note that this article uses the term "lift" throughout, but in the actual aerodynamic computations, axial force and normal force are computed and then lift and drag are computed from them.)

The latest version of the aeroprediction code[2-4] (referred to here as OAP) calculates the linear lift of the body alone with empirical methodology in subsonic and transonic flow,[5] with the hybrid theory in low supersonic flow of Van Dyke,[6] the theory in moderate supersonic flow of DeJarnette et al.,[7] and the recent work in hypersonic flow of Moore et al.[8] The nonlinear body lift is estimated by the Allen-Perkins viscous crossflow theory[9] in all speed regimes. The linear lift of the wing alone is predicted by lifting surface theory in subsonic flow,[10] three-dimensional thin-wing theory in supersonic flow,[11] and an empirical method for blending the two in transonic flow.[12] Two-dimensional strip theory was used for hypersonic flow.[4] No nonlinear component of wing-alone lift is accounted for in the OAP. There is an option for high angle-of-attack total configuration lift prediction based on an older high angle-of-attack database.[13] However, the configurations considered are more limited than desired, and the method used overlaps with the linear lift portion of the present component buildup approach used in the aeroprediction code. For this reason, a new approach for estimating nonlinear wing-alone and wing-body lift that is compatible with a component buildup approach is desired.

In investigating the literature for available nonlinear component buildup approaches, the authors found several alternatives.[13-20] However, most of these alternatives estimated the total lift including the linear term in an empirical or semiempirical manner. Those methods either did not separate the lift into a linear term and a nonlinear term[19,20] or were more limited in Mach number or configurations than desired.

The present new approach is a blend, to some extent, of the methods discussed in Refs. 13–15 and 18–20. It divides the lift into a linear term and a nonlinear term analogous to Refs. 19 and 20. It emphasizes low aspect ratios as does Ref. 18. Finally, it uses the large databases of Refs. 13–17 to estimate the nonlinear and interference lift terms that are compatible with the linear lift and interference terms predicted by linear theories or slender body theory.

The new method has several advantages over existing techniques. Other than the theory of Ref. 20, it is the only technique compatible with existing codes that use linearized theory for lift. Unlike Ref. 20, it includes the entire Mach number, aspect ratio, and taper ratio ranges. It includes the physics of the lower Mach number, strong aspect ratio dependence of the nonlinear lift, and high Mach number compressibility effects. Finally, it limits itself to planar aerodynamics and does not carry in computer storage of the large database associated with roll-dependent aerodynamics. So, although the new method is being designed to be complementary to the NSWCDD aeroprediction code, it is general enough to be easily incorporated into other linearized lift codes.

Analysis

This paper summarizes the new methods for calculating nonlinear lifting properties on missile configurations. For the details of the new methods, interested readers are referred to Ref. 21, which is a comprehensive report including several hundred comparisons of the new methods with experimental data and other theoretical techniques.

Wing-Alone Lift

The methodology in the OAP for predicting linearized lift uses three-dimensional thin-wing theory for supersonic Mach numbers, lifting surface theory for subsonic Mach numbers, and an empirical technique to blend the supersonic and subsonic methodologies together in the transonic region.[22] This process works reasonably well for wings of aspect ratio 1 and higher. However, as aspect ratio gets small, the aforementioned methodology fails for several reasons. First, it was assumed that Mach lines emanating from a wing tip did not alter the pressure distribution and hence aerodynamics of an opposite wing. As aspect ratio gets small, this assumption is violated, and account must be taken of the opposite wing side edge effects. Second, in comparing the low aspect ratio theory with experimental data,[16] the theoretical X_{cp} is too far forward for the low aspect ratio rectangular (or nearly rectangular) surfaces. A third problem concerns low aspect ratio wings in subsonic flow. The OAP was designed for aspect ratios of 1 and higher; thus, the number of points on the wing surface was four in the chordwise and three in the spanwise direction. Inaccurate results are therefore expected as aspect ratio gets small. To remedy one of these problems, the linearized lifting theory of Evvard,[23] which allows opposite wing tip effects to be included in the aerodynamic computations, has been implemented. The other two problems were dealt with by assuming an override in the linear theory for wing lift and X_{cp} for certain values of λ, AR, and M_∞. This override was based on experimental data.

The total lift of the wing is

$$C_N = C_{N_L} + C_{N_{NL}} \tag{1}$$

where $C_{N_{NL}}$ is a nonlinear term of the form

$$C_{N_{NL}} = f(M_N, AR, \lambda)\left(\frac{A_p}{A_{\text{ref}}}\right)\sin^2\alpha \tag{2}$$

Equation (2) is of the same form as the Allen-Perkins[9] viscous crossflow methodology for bodies except that the product ηC_{d_c} has been replaced by $f(M_N, AR, \lambda)$.

To get a feel for how to derive the coefficient in Eq. (2), several wing-alone lift curve slopes were examined for various values of aspect ratio using the databases of Refs. 14–16 and a full Euler code solution.[24]

At low-to-moderate values of aspect ratio typical of those used on most missiles, C_{N_α} will typically increase as angle of attack increases. This increase is larger with the smaller aspect ratio wings where the linear lift term is smallest (C_{N_α} approaches $\pi/2$ AR). At high aspect ratio where the linear lift term approaches its two-dimensional value of 2π, the nonlinear lift with angle of attack greater than about 10–15 deg is typically negative. In all cases, there is a noticeable effect of compressibility for large values of M_N.

To model these two effects, one mainly due to planform shape and the other due to compressibility, use has been made of the large wing-alone databases of Refs. 14–16. Values of the function $f(M_N, AR, \lambda) = k_1$ of Eq. (2) were computed using the experimental databases and the linear wing-alone lift curve slopes predicted by the aeroprediction code.[2-4] That is, from the experimental data, values of the total wing-alone normal force are known. From the linearized theories used in the aeroprediction code, C_{N_L} values are known for the same set of freestream conditions and wing parameters. From these two values

$$C_{N_{NL}}(M_N, AR, \lambda) = C_N(M_N, AR, \lambda) - C_{N_L}(M_N, AR, \lambda) \tag{3}$$

From these values of $C_{N_{NL}}$, k_1 can be computed as

$$k_1 = \frac{C_{N_{NL}}(M_N, AR, \lambda)}{\sin^2\alpha} \tag{4}$$

Values of k_1 for all of the conditions available in the experimental data sets of Refs. 14–16 were computed and are given

Table 1 Values of k_1 for lower Mach numbers ($\alpha \leq 30$ deg)

λ/M_∞	0.0	0.5	1.0	1.5	2.0	2.5	3.0	3.5	4.0	4.5
$AR \leq 0.5$, $M_\infty < 4.0$										
0.0	1.55	1.57	1.60	1.60	1.51	1.25	0.92	0.56	0.29	0.16
0.5	2.84	2.90	2.82	2.30	1.35	1.00	0.80	0.64	0.47	0.33
1.0	2.37	2.45	2.43	2.31	1.50	1.05	0.90	0.75	0.61	0.48
$AR = 1.0$, $M_\infty < 3.5$										
0.0	1.32	1.48	1.46	0.99	0.40	0.22	0.12	0.09	0.09	0.11
0.5	2.44	2.45	1.85	0.70	0.31	0.19	0.20	0.26	0.36	0.43
1.0	1.20	1.22	1.10	0.50	0.45	0.50	0.65	0.78	0.88	0.94
$AR \geq 2.0$, $M_\infty < 3.5$										
0.0	−1.80	−1.84	−1.95	−1.20	−0.20	−0.09	−0.06	−0.03	0.11	0.18
0.5	−1.80	−1.84	−1.95	−1.20	−0.20	0.30	0.41	0.60	0.72	0.80
1.0	−1.45	−1.47	−1.35	−0.70	0.20	0.60	0.83	0.98	1.09	1.15

Table 2 Values of k_1 for higher Mach numbers ($\alpha \leq 30$ deg)

$\lambda/M_\infty \sin\alpha$	0.0	0.5	1.0	1.5	2.0	2.5	3.0	3.5	4.0	4.5	5.0	5.5	6.0
$AR \leq 0.5$, $M_\infty \geq 4.0$													
0.0	−1.60	−0.98	0.23	0.55	0.71	0.82	0.89	0.92	0.95	0.95	0.95	0.95	0.95
0.5	−0.87	−0.24	0.33	0.60	0.73	0.82	0.89	0.92	0.95	0.95	0.95	0.95	0.95
1.0	−0.31	0.09	0.46	0.68	0.78	0.87	0.91	0.93	0.95	0.95	0.95	0.95	0.95
$AR = 1.0$, $M_\infty \geq 3.5$													
0.0	−0.39	−0.39	−0.29	0.06	0.29	0.48	0.60	0.69	0.75	0.81	0.86	0.91	0.94
0.5	0.14	0.17	0.29	0.46	0.63	0.76	0.85	0.90	0.93	0.95	0.95	0.95	0.95
1.0	0.30	0.50	0.86	0.93	0.94	0.95	0.95	0.95	0.95	0.95	0.95	0.95	0.95
$AR \geq 2.0$, $M_\infty \geq 3.5$													
0.0	−0.25	−0.09	0.15	0.8	0.91	0.95	0.95	0.95	0.95	0.95	0.95	0.95	0.95
0.5	0.02	0.29	0.80	0.98	0.98	0.97	0.97	0.96	0.95	0.95	0.95	0.95	0.95
1.0	0.66	1.02	1.15	1.18	1.15	1.09	1.02	0.96	0.95	0.95	0.95	0.95	0.95

in Tables 1 and 2. Table 1 is for the lower speed conditions where crossflow compressibility effects are small and wing aspect ratio is the dominant effect. Here, values of k_1 are averaged over the angle-of-attack range of 0–30 deg. For the higher Mach numbers, it was more convenient to plot the k_1 vs M_N rather than M_∞ (see Table 2). In so doing, the k_1 approached a value of 0.95 for high values of M_N. This agrees very well with the crossflow drag coefficient of 1.72 of Ref. 25 and the value of η for a wing of 0.55 of Ref. 26. The product of these two, $\eta C_{d_c} = 0.95$, shows that at high Mach numbers the wing-alone nonlinear lift term is similar to that of the body alone. However, at lower Mach numbers the crossflow drag coefficient apparently varies considerably for the various planforms, and therefore Tables 1 and 2 are needed.

The center of pressure and pitching moment of the linear component of lift are computed in a manner similar to that in Ref. 21. The center of pressure of the nonlinear component of lift is assumed to be at the center of the planform area. The total center of pressure of the wing alone is also assumed to vary linearly between its linear theory value near $\alpha = 0$ to the nonlinear value (centroid of wing planform area) at $\alpha = 45$ deg. In equation form, this assumption states

$$X_{cp} = (X_{cp})_L + \frac{\alpha}{45}\left[(X_{cp})_{NL} - (X_{cp})_L\right] \tag{5}$$

where

$$(X_{cp})_{NL} = X_{WA} \tag{6}$$

The total wing-alone pitching moment is then

$$C_M = -C_N X_{cp} \tag{7}$$

Improved Body-Alone Nonlinear Lift

The body-alone linear lift is determined by the hybrid theory of Van Dyke or the second-order shock-expansion theory for the $M_\infty \geq 1.2$ region and by empirical estimates in the subsonic and transonic speed regimes ($M_\infty < 1.2$). The nonlinear lift of the OAP is estimated using the Allen-Perkins viscous crossflow theory.[9] This theory states that

$$(\Delta C_N)_{NL} = \eta C_{d_c} \frac{A_p}{A_{\text{ref}}} \sin^2\alpha \tag{8}$$

where η is given by Fig. 1a and C_{d_c} by Fig. 1b. In Fig. 1b, no account was taken for variations in C_{d_c} with Reynolds number because past experience in using this theory had not shown a need to do so. The center of pressure of the nonlinear lift term was assumed to occur in the crossflow plane at the center of the planform area. The overall body-alone center of pressure is therefore dependent on the center of pressure of the linear lift term combined with the nonlinear lift center of pressure. The moment about a given point X_0 is then

$$C_M = -C_N(X_{cp} - X_0) \tag{9}$$

where C_M is assumed to be positive in the nose-up direction.

Three modifications were made to the previous methodology. The first is a slight change in the values of C_{d_c}. The values used in the OAP were based on the ¼-in. scale diameter model of Ref. 9. The improved aeroprediction code (IAP) uses the data in the same reference but for various diameters. This change mainly affects the values of C_{d_c} for values of $M_N < 2.5$. The new values of C_{d_c} are as much as 50% lower than the old values. For crossflow Mach numbers less than 0.45, Ref. 9 had no various diameter data, so the database of Ref. 17 was used to help define C_{d_c} for M_N values less than 0.45. The OAP and IAP values of C_{d_c} are shown in Fig. 1b.

The second change to the body-alone nonlinear lift prediction methodology is in the value of η. The OAP assumes no variation of η with crossflow Mach number. However, the data of Ref. 26 indicate a significant effect as the crossflow Mach number becomes supersonic. The data from Ref. 26 are

repeated in Fig. 1c. Also shown in Fig. 1c is the current assumed representation of these data. The dashed line in Fig. 1c is defined by

$$\eta = \left(\frac{1-\eta_0}{1.8}\right)M_N + \eta_0 \quad \text{for} \quad M_N \leq 1.8$$
$$\eta = 1 \quad \text{for} \quad M_N > 1.8 \tag{10}$$

where η_0 is the value of η from Fig. 1a, and M_N is the crossflow Mach number. It was also found that as the freestream Mach number approaches moderate supersonic values, a value of $\eta = 1.0$ should be used for all computations involving Eq. (8) for the body alone. A value of $M_\infty = 2.75$ is being used in the IAP.

The third change in the body-alone nonlinear lift prediction is in the center of pressure. The OAP assumes that the linear term center of pressure computed at low angle of attack remains constant at all angles of attack and is combined with the nonlinear lift term at high angles of attack. It was found that this assumption gave a center of pressure slightly more unstable (closer to the nose tip) than data suggest for low subsonic and moderate-to-high supersonic Mach numbers. It is suspected that the center of pressure of the linear term shifts rearward with angle of attack. To correct this, a constant shift in the center of pressure of 3% of the body length rearward was assumed for angles of attack of 10 deg and greater at Mach numbers of 0.6 and less or 2.0 and greater.

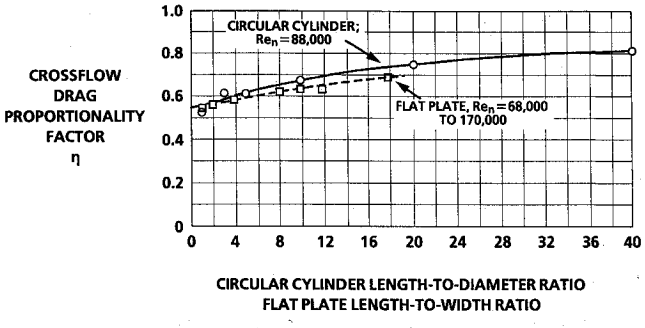

Fig. 1a Ratio of crossflow drag coefficient for a finite length cylinder (or flat plate) to that for an infinite-length cylinder (or flat plate) (taken from Ref. 26).

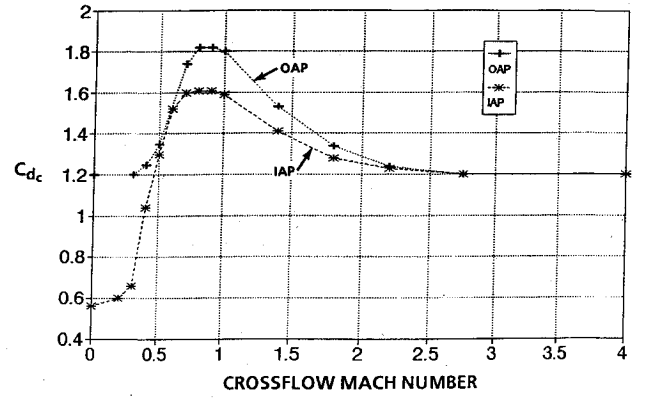

Fig. 1b Crossflow drag coefficient for an ogive-cylinder configuration.

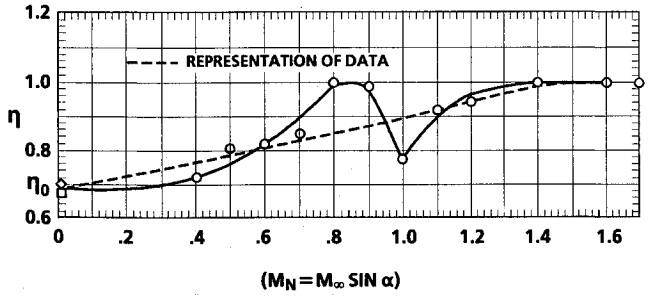

Fig. 1c Variation of η with M_N obtained from experiment (taken from Ref. 26).

Nonlinear Wing-Body Interference

The total configuration normal force coefficient at a given angle of attack, control deflection, and Mach number is[27]

$$C_N = C_{N_B} + \{[K_{W(B)} + K_{B(W)}]\alpha + [k_{W(B)} + k_{B(W)}]\delta_W\}(C_{N_\alpha})_W + \{[K_{T(B)} + K_{B(T)}]\alpha + [k_{T(B)} + k_{B(T)}]\delta_T\}(C_{N_\alpha})_T + C_{N_{T(V)}} \tag{11}$$

The first term in Eq. (11) is the normal force of the body alone, including the linear and nonlinear components; the second term is the contribution of the wing (or canard), including interference effects and control deflection; the third term is the contribution of the tail, including interference effects and control deflection; and the last term is the negative downwash effect on the tail due to wing shed or body shed vortices. The various K represent the interference of the configuration with respect to angle of attack, and the various k represent the interference with respect to control deflection. Each of these interference factors is estimated in the OAP by slender body theory (SBT) or linear theory (LT) as discussed in Ref. 27. As such, they are independent of angle of attack. What is desired is to estimate the change in these parameters with angle of attack. To do this, use will once again be made of the large databases of Refs. 14–17.

Before discussing the interference factor empirical model for high angle of attack, a brief discussion of the databases being used is appropriate. Figure 2 gives a summary of all three databases, including a list of problems in trying to use all three databases simultaneously in developing empirical models. The two most important problems are the differences in wing-alone normal force between the database of Ref. 14 and that of Ref. 16 and the small wing areas for aspect ratio of 2 and greater used in the database of Ref. 17. This latter problem means that it is more difficult to get accurate body-wing interference lift values. The former problem required discretion as to which data to use, and the data of Ref. 16 were given more weight in developing the interference models. It should also be mentioned that, although 8 of 11 planforms were the same between Refs. 16 and 17, the thickness and airfoil shapes were different, which can give slight differences in aerodynamics as well.

Of the interference factors affected by angle of attack, $K_{W(B)}$ or $K_{T(B)}$ and $K_{B(W)}$ or $K_{B(T)}$ are by far the most important. Reference 14 showed that $k_{W(B)}$ or $k_{T(B)}$ had only a slight angle-of-attack effect up to $\alpha =$ 25 deg or δ up to 40 deg. As a result, it is assumed that $k_{W(B)}$ and $k_{T(B)}$ are independent of angle of attack and will be estimated as present in the OAP from SBT or LT. This same assumption is made for the interference lift on the body due to control deflection $k_{B(W)}$ or $k_{B(T)}$.

Returning to the factor $K_{W(B)}$ or $K_{T(B)}$, data from Refs. 14–17 have been plotted as a function of angle of attack for several Mach numbers, aspect ratios, and taper ratios.[21] Typical of these data are the results given in Fig. 3, which gives the experimental value of $K_{W(B)}$ as a function of angle of attack for various values of AR and λ and at $M_\infty = 4.6$. These curves, along with others in Ref. 21, were generated by subtracting the body-alone lift from the wing-body lift of Ref. 17, then dividing by the wing-alone lift of Ref. 14 or Ref. 16 depending on Mach number. Several points are worthy of note. First, there is some scatter in the data particularly at $M_\infty \leq 0.8$, so one must use the data as a guide in making empirical correlations. Second, even though there is scatter in the data, all of the curves exhibit the general trend shown in Fig. 4. That is, for low angles of attack, the data seem to say that slender body

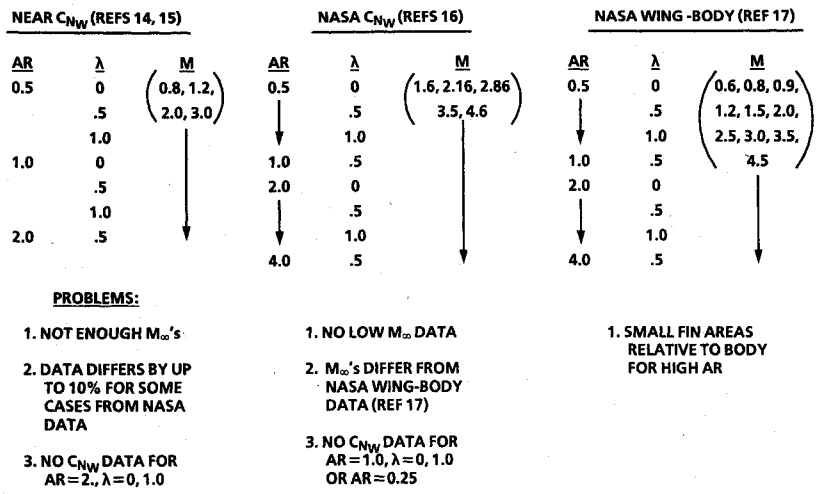

Fig. 2 Summary of databases used for $K_{W(B)}$ and $K_{B(W)}$.

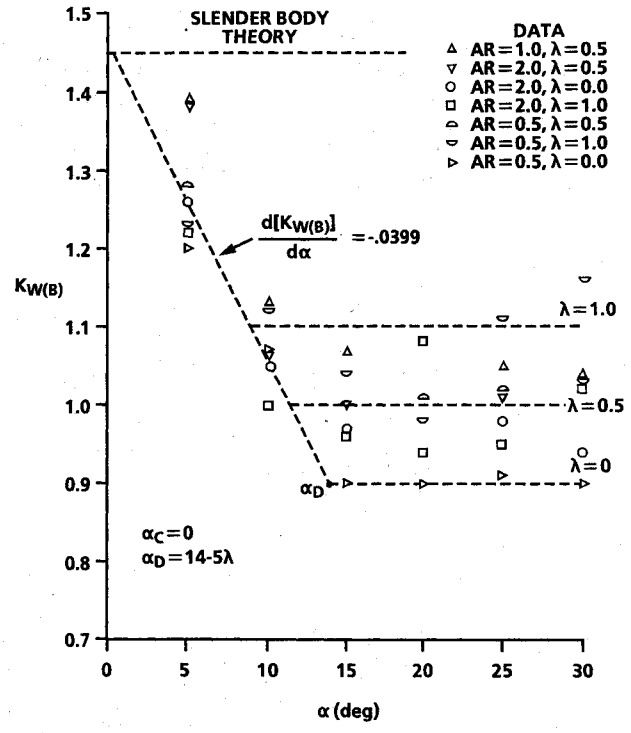

Fig. 3 Wing-body interference factor based on experimental data ($M_\infty = 4.6$).

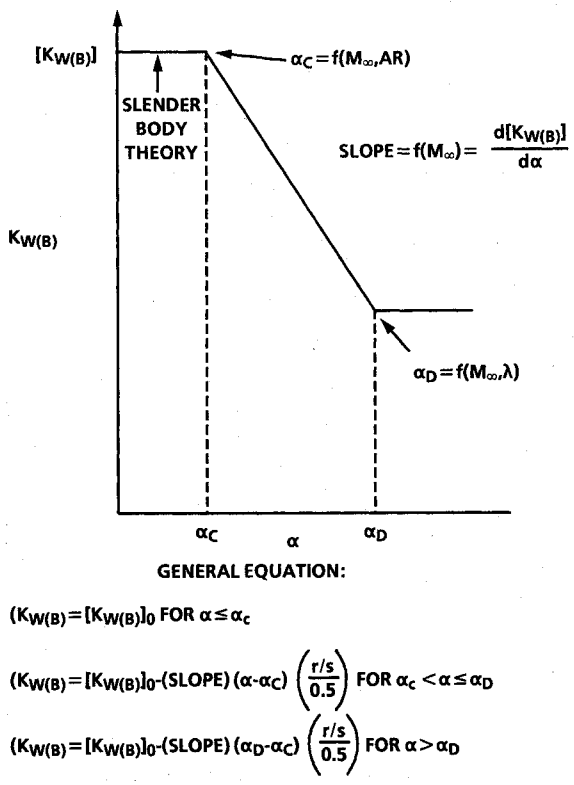

Fig. 4 Qualitative behavior of wing-body interference factor as a function of angle of attack.

theory is a good estimate of $K_{W(B)}$. As angle of attack increases, $K_{W(B)}$ decreases from its slender body value. This decrease starts at some angle defined as α_c in Fig. 4, which is primarily a function of aspect ratio and Mach number. The $K_{W(B)}$ then decreases in a nearly linear fashion. The slope of this linear decrease appears to be primarily a function of Mach number. Finally, a minimum value of $K_{W(B)}$ is reached, which appears to be a function of Mach number and taper ratio. Although all of the data of Fig. 3 are for r/s values of 0.5, SBT says that $K_{W(B)}$ varies nearly linearly with r/s. Hence, the equations in Fig. 4, which represent the three segments of the curves in Fig. 4, also make this assumption.

An attempt was made to arrive at empirical estimates of α_c, slope, and α_D. If this could be done, an empirical model based on the current theory in the aeroprediction code could be made without resorting to large data storage and table lookup and interpolations. Figures 5–7 show these results. Figure 5 shows that the slope of the decrease in $K_{W(B)}$ varies approximately linearly with Mach number. As shown in the figure, as Mach number increases, the value of $K_{W(B)}$ decreases more rapidly as evidenced by the larger negative values of the slope. Reference 14 indicates shock wave interactions as a likely cause of this phenomenon. Figure 5 also shows the increment in $[\Delta K_{W(B)}]_\alpha = 0$, which occurs at low Mach numbers.

Figure 6 shows the results of the value of α_c, the point where $K_{W(B)}$ starts its decline, as a function of Mach number and aspect ratio. Taper ratio dependence was only slight and was therefore neglected. Figure 6 shows that as Mach number increases, α_c decreases to zero. That is, $K_{W(B)}$ starts decreasing immediately, even at small angles of attack, from its slender body value. Figure 6 also shows that α_c decreases with increasing aspect ratio. Approximate equations for estimating α_c are given in the figure.

Finally, Fig. 7 shows a fairly consistent general trend of α_D as a function of taper ratio and Mach number. The mathematical model for α_D is also shown in the figure. Since there were

no data past $M_\infty = 4.6$, the curves were extrapolated to $M_\infty = 5$. If $M_\infty > 5$, it was assumed that the values for α_D were the same as those for $M_\infty = 5$. It is not known how good this assumption is. However, it will allow the code to compute a number for $M_\infty > 5$ and hence compute total force and moments.

The general empirical model for estimating nonlinear wing-body interference $K_{W(B)}$ or $K_{T(B)}$ is therefore given by the equations in Fig. 4 where

$$[\Delta K_{W(B)}]_{\alpha=0}, \quad \alpha_c, \quad \frac{dK_{W(B)}}{d\alpha}, \quad \text{and} \quad \alpha_D$$

are found from Figs. 5–7.

This empirical model is for angles of attack less than 30 deg and cruciform missile configurations in the plus (or $\phi = 0$ deg) roll orientation. At angles of attack greater than 30 deg (or 25 deg in some instances), the assumption of a constant value of $K_{W(B)}$ for values of α greater than α_D becomes less accurate.

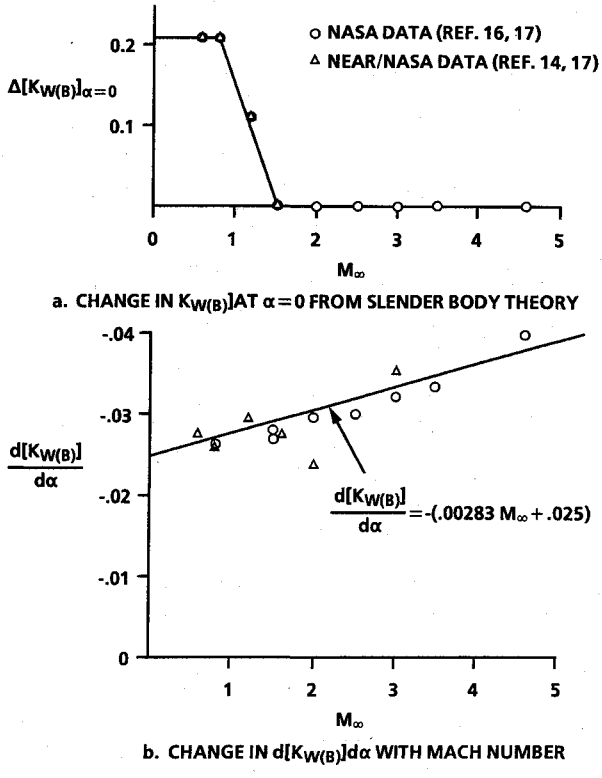

Fig. 5 Parameters used in nonlinear wing-body interference model.

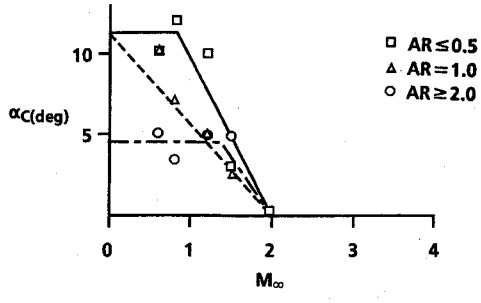

MODEL

IF $M_\infty \geq 2, \alpha_C = 0$

IF $M_\infty < 2$,

$\alpha_C = 12.5 - 1.06\ M_\infty - 2.59 M_\infty^2$	FOR AR≤0.5
$\alpha_C = 12.5 - 6.25\ M_\infty$	FOR AR=1.0
$\alpha_C = 4.5 + 2.25\ M_\infty - 2.25 M_\infty^2$	FOR AR≥2.0

Fig. 6 Model for the angle where the wing-body interference factor starts decreasing as a function of the various parameters.

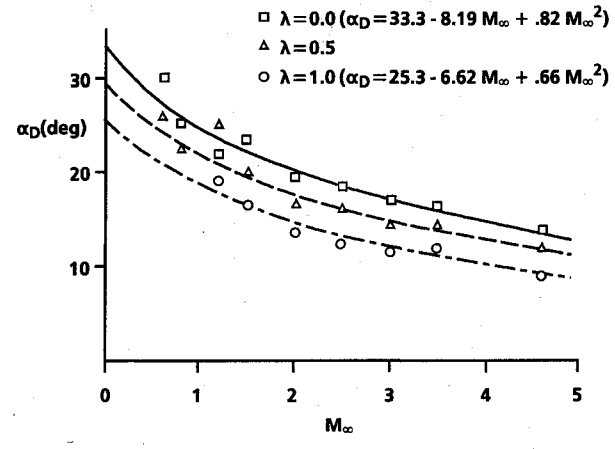

Fig. 7 Change in angle where wing-body interference factor reaches a minimum.

Data actually show that $K_{W(B)}$ starts increasing again with larger values of α. Since the aeroprediction code is a planar code and oriented to angles of attack less than 30 deg, this variation was neglected. Although an assumption has been made to allow computations greater than $M_\infty = 5.0$, the database itself only goes to $M_\infty = 4.6$.

Nonlinear Body-Wing Interference

As discussed previously, the two main interference terms of concern with respect to angle-of-attack effects are the wing-body and body-wing interference terms. This section deals with the change in the body-wing interference factor with angle of attack. The NASA Tri-Service Data Base is again used to estimate this parameter.[14–17] The database of Ref. 17 was taken with two independent balance measurements where one balance measured the forces on the body, whereas the other measured the forces on the wing. This way the lift of the wing in the presence of the body and the lift of the body in the presence of the wing could be measured. The $K_{B(W)}$ is defined as

$$K_{B(W)} = \frac{\Delta C_{NB(W)}}{C_{N_W}} \tag{12}$$

The $\Delta C_{N_{B(W)}}$ is computed from the total wing-body normal force database of Ref. 17 by the following process:

$$\Delta C_{N_{B(W)}} = C_{N_{\text{TOTAL}}} - 2C_{N_{W(B)}} - C_{NB} \tag{13}$$

Twice the wing-body normal force coefficient is used in Eq. (13) because only one fin was included in the measurements. The C_{N_W} of Eq. (12) comes from the wing-alone databases of Ref. 14 or Ref. 16. In obtaining C_{N_W} at the Mach numbers of the database of Ref. 17, some interpolation and extrapolation were needed to obtain normal force coefficients at the Mach numbers and angles of attack of Ref. 17. Again, only the planar roll case ($\phi = 0$ deg) was considered, although the database of Ref. 17 included all roll positions.

In performing the previous computations, two problems were noted. The first had to do with the fact that the database of Ref. 17 kept wing span constant while varying AR and λ. This allowed the wing area to vary. These areas (for one fin) varied from 0.125 to 0.0078125 ft^2. On the other hand, the database of Ref. 16 maintained a constant wing area while varying AR and λ. Thus, for the smaller fins of Ref. 17, the inaccuracies associated with wind-tunnel measurements and subtraction of numbers in Eq. (13) yield results that are expected to have much more scatter than those where the wing area is a reasonable size compared with the body cross section. The data for AR of 1 and less are therefore believed to be of better accuracy than those for AR of 2 and greater. The

second problem was similar to the previous one except it was Mach number dependent. It was found that as M_∞ gets to moderate supersonic Mach numbers, the $\Delta C_{N_{B(W)}}$ approaches zero fairly rapidly with angle of attack. Hence, the absolute value of $K_{B(W)}$ is more suspect under these conditions as well.

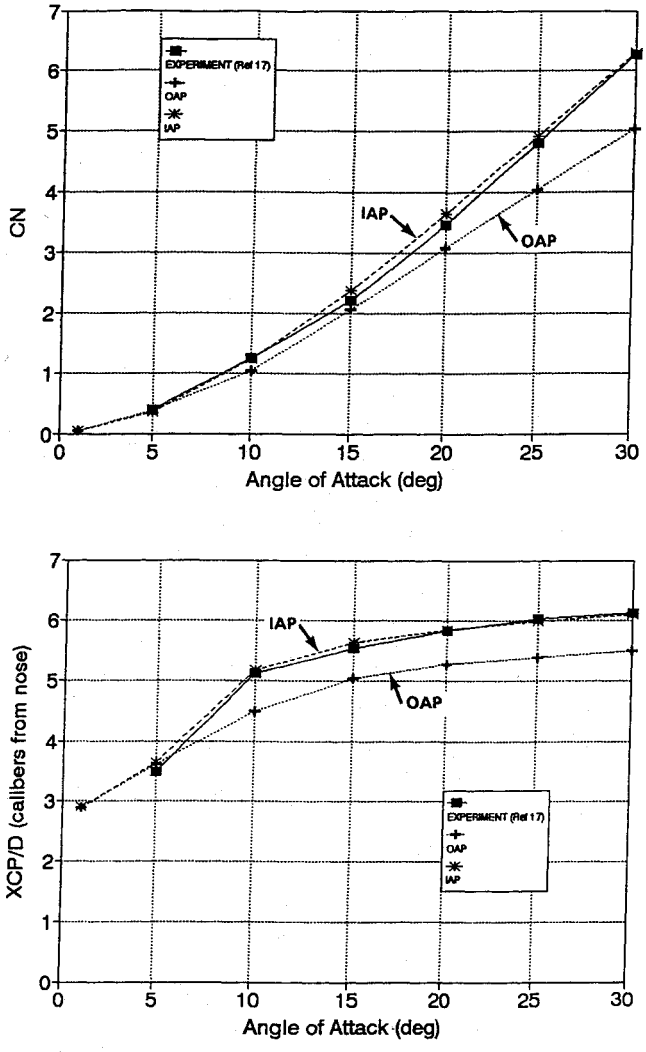

Fig. 8 Body-alone normal force coefficient and center of pressure ($M_\infty = 3.5$).

In developing a semiempirical model using the databases of Refs. 14–17 as well as the SBT and LT of the OAP, an equation of the form

$$K_{B(W)} = [K_{B(W)}]_{\text{OAP}} \frac{+r/s}{0.5} \left\{ [\Delta K_{B(W)}]_{\alpha=0} + \frac{\mathrm{d}[K_{B(W)}]}{\mathrm{d}\alpha} |\alpha| \right\} \tag{14}$$

was found to represent the data reasonably well. Here the first term is the value from the SBT and LT of the OAP. The factor $(r/s)/0.5$ of the second term represents the fact that the data were obtained at r/s values of 0.5, and a linear variation is assumed in the second term with r/s. This is similar to the variation experienced by the SBT.[28] The first term in the brackets of the second term is the difference between the OAP and experimental data at $\alpha = 0$. The second term in the brackets is the change in the value of $K_{B(W)}$ with angle of attack based on the experimental databases.

To compute the last two terms

$$[\Delta K_{B(W)}]_{\alpha=0} \quad \text{and} \quad \frac{\mathrm{d}[K_{B(W)}]}{\mathrm{d}\alpha}$$

values of these parameters were computed for each Mach number and are given in Table 3. Note that since data were available for $0.6 \le M_\infty \le 4.5$ only, outside these regions values of the parameters were either assumed as the values at $M_\infty = 0.6$ or 4.5 or extrapolated past these values. Also, cutoffs in the values of $K_{B(W)}$ were assumed that did not allow the value to go below zero or to increase past the SBT value of 2.0. To use the data of Table 3, a three-parameter linear interpolation for the two parameters is performed as a function of λ, AR, and M_∞.

The center of pressure for the body-wing nonlinear interference lift is assumed to be at the same point as the linear term of the lift. This value is computed in the OAP using LT with and without afterbody sections for supersonic Mach numbers. For subsonic flow, it is assumed to be located at the center of pressure of the wing-alone lift. In transonic flow, the center of pressure is assumed to vary linearly between its value at $M_\infty = 1.2$ and the subsonic value.

Results and Discussion

Configuration Components

To develop an accurate semiempirical, nonlinear, lift model for high angles of attack, it is important to validate the model as much as possible on individual components before validation of total configuration aerodynamics takes place. Validation of individual components can be done with experimental

Table 3 Data for body-wing nonlinear semiempirical interference model

		Mach number								
AR	λ	≤0.6	0.8	1.2	1.5	2.0	2.5	3.0	3.5	≥4.5
$[\Delta K_{B(W)}]_{\alpha=0}$										
≤0.25	0, 0.5, 1.0	−0.1	−0.1	0.5	0.6	0.7	0.8	0.7	0.5	0.3
0.5	0.5	−0.28	−0.1	0.13	0.11	0.05	−0.02	−0.06	0	0
1.0	0.5	−0.26	−0.2	0.15	0.21	0.15	0	0	0	0
≥2.0	0.5	−0.13	−0.04	0.12	0.43	−0.16	0	0.37	−0.08	−0.16
0.5	0	−0.3	−0.06	0.26	0.28	0.17	0.12	0.14	0	0
≥2.0	0	−0.2	−0.1	0.12	0.52	0.12	0.15	0.22	−0.06	−0.22
0.5	1.0	−0.16	0.08	0.26	0.14	−0.12	0	−0.05	−0.10	0
≥2.0	1.0	−0.2	−0.1	0.12	0.45	−0.02	0.11	0.28	−0.17	−0.3
$\mathrm{d}[K_{B(W)}]/\mathrm{d}\alpha$										
≤0.25	0, 0.5, 1.0	0.018	0.013	−0.010	−0.023	−0.013	−0.022	−0.031	−0.025	−0.031
0.5	0.5	0.019	0.010	−0.008	−0.010	−0.013	−0.013	−0.013	−0.012	−0.012
1.0	0.5	0.013	0.010	−0.007	−0.013	−0.020	−0.017	−0.012	−0.012	−0.012
≥2.0	0.5	0.010	0.011	0	−0.013	−0.010	−0.017	−0.040	−0.012	−0.012
0.5	0	0.033	0.022	0	−0.007	−0.010	−0.008	−0.014	−0.012	−0.012
≥2.0	0	0.010	0.010	−0.007	−0.020	−0.011	−0.020	−0.023	−0.012	−0.012
0.5	1.0	0.019	0	−0.019	−0.010	−0.007	−0.013	−0.014	−0.012	−0.012
≥2.0	1.0	0.010	0.01	−0.007	−0.017	0	−0.017	−0.026	−0.012	−0.012

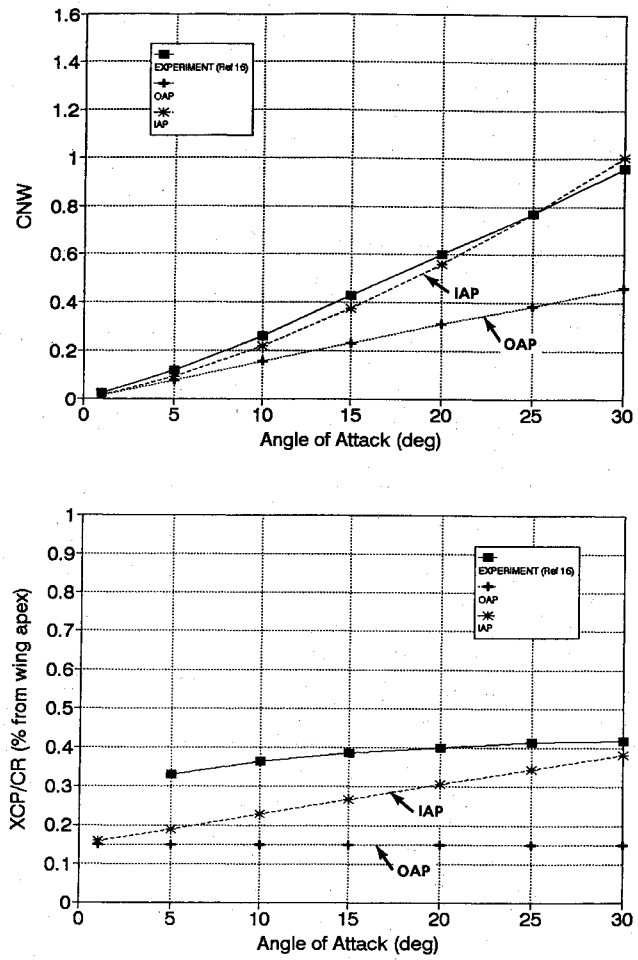

Fig. 9 Wing-alone normal force coefficient and center of pressure ($AR = 0.5$, $\lambda = 1.0$, $M_\infty = 1.6$).

data or more accurate numerical codes. For the methodology developed herein, validation of the body alone, wing alone, and wing-body and body-wing interference lift components will be treated separately. The large databases of Refs. 14–17 will be the main source of data comparison. Only a sample of the several hundred cases presented in Ref. 21 will be shown.

Figure 8 presents typical results of the new semiempirical model for the body-alone normal force coefficient and center of pressure for $M_\infty = 3.5$ as a function of angle of attack. The body is 12.33 calibers long with a 3-caliber tangent ogive nose. This is the same model of the database in Ref. 17. The IAP normal force coefficient results show significant improvement over those of the OAP. Although this figure is for $M = 3.5$, Ref. 21 shows that this statement is true at just about all conditions considered. The areas of most significant improvement are at low Mach numbers where C_{d_c} was reduced significantly from the OAP results and at high Mach number where the OAP did not account for compressibility effects on η.

Center of pressure comparisons of Fig. 8 (and other cases in Ref. 21) show improvement of the IAP results over the OAP results when compared with experiment and full Euler computations. However, the improvement is not as great as with the normal force. In fact, at some Mach number and angle-of-attack conditions, IAP results are not as accurate as OAP results. This occurs primarily at transonic and lower supersonic Mach numbers. At low angles of attack, the discrepancy between the IAP and experiment can be as high as 8% of the body length. One should keep in mind, however, that this is the area for greatest scatter in the experimental data. For other Mach numbers and angles of attack, the agreement between experiment and the IAP is quite impressive.

In general, it is believed that the IAP body-alone nonlinear normal force prediction is much improved over the OAP results. The center of pressure is also better for the IAP vs the OAP when viewed over all conditions considered.

Typical results of the new wing-alone model are shown in Fig. 9 for $AR = 0.5$ and $\lambda = 1.0$. Results are given in terms of normal force coefficient and center of pressure for $M_\infty = 1.6$ and as a function of angle of attack. As seen in the figure, the IAP shows significant improvements over the OAP on C_N prediction and some improvement in X_{cp} prediction.

In examining other cases of Ref. 21, the IAP shows significant improvement over the OAP on normal force prediction compared with experiment at just about all values of M_∞, AR, α, and λ considered. The areas of greatest improvement are at high α and low aspect ratio, although other aspect ratios also have substantial improvement. The IAP shows some slight improvement over the OAP in center of pressure prediction when compared with experiment. The most notable improvements are at low Mach number, low aspect ratio, and $\lambda \geq 0.5$. The reason for the lack of more significant improvement in the center of pressure prediction is that experiment has thickness included and both the OAP and IAP assume a flat plate for lift prediction. The thickness effect could be included by combining the axial pressure prediction with the normal force prediction to get a new center of pressure based on these combined effects. However, due to funding and time constraints, this was not done.

To summarize the wing-alone nonlinear prediction, the new IAP methodology shows substantial improvements over the OAP on normal force coefficient prediction and slight improvements in center of pressure compared to experiment.

Typical results for the wing-body and body-wing interference are presented in Fig. 10. Figure 10 presents the results in

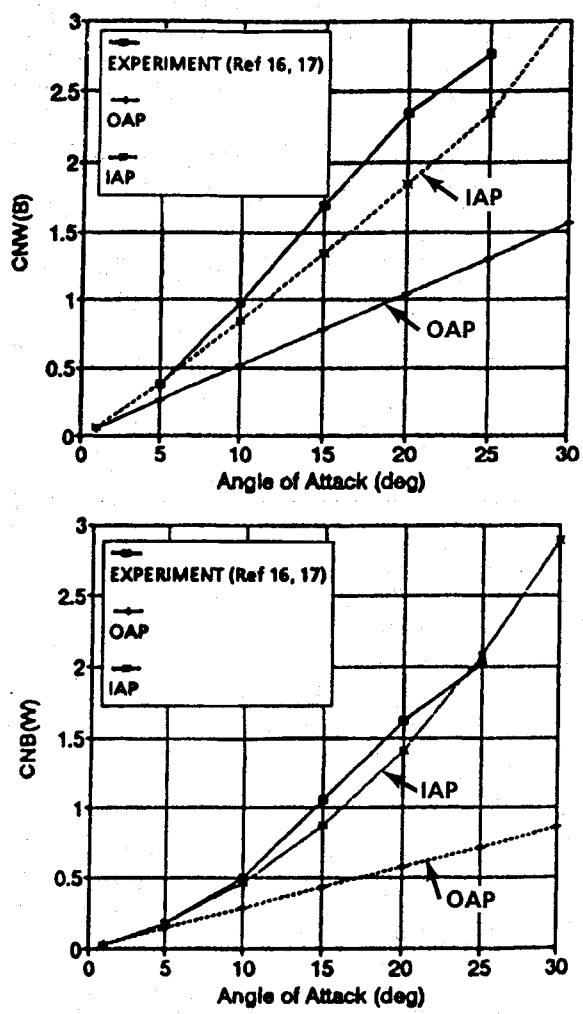

Fig. 10 Wing-body and body-wing interference as a function of angle of attack ($AR = 0.5$, $\lambda = 0.5$, $M_\infty = 0.8$).

terms of the total normal force coefficient on the wing in the presence of the body $C_{N_{W(B)}}$, and additional normal force coefficient on the body generated by the presence of the wing $C_{N_{B(W)}}$. The case is for $M_\infty = 0.8$ and $AR = \lambda = 0.5$. Note that

$$C_{N_{W(B)}} = K_{W(B)}\, C_{N_W} \frac{A_W}{A_{\text{ref}}} \tag{15}$$

$$C_{N_{B(W)}} = K_{B(W)}\, C_{N_W} \frac{A_W}{A_{\text{ref}}} \tag{16}$$

Although only 1 of 63 cases in Ref. 21 has been shown, the results are fairly typical. In general, the IAP interference lift terms show substantial improvement over the OAP at just about all conditions of angle of attack, Mach number, aspect, and taper ratio considered. The areas of greatest improvement are at low Mach number and low aspect ratio, but other conditions also show significant improvement. It should be pointed out that the Figs. 8–10 comparisons are for cases within the database from which the empirical model was derived.

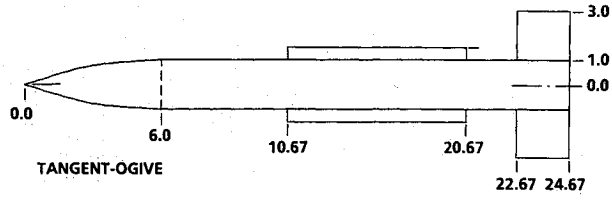

Fig. 11a Body-dorsal-tail configuration used for comparing ZEUS, IAP, and OAP computations.

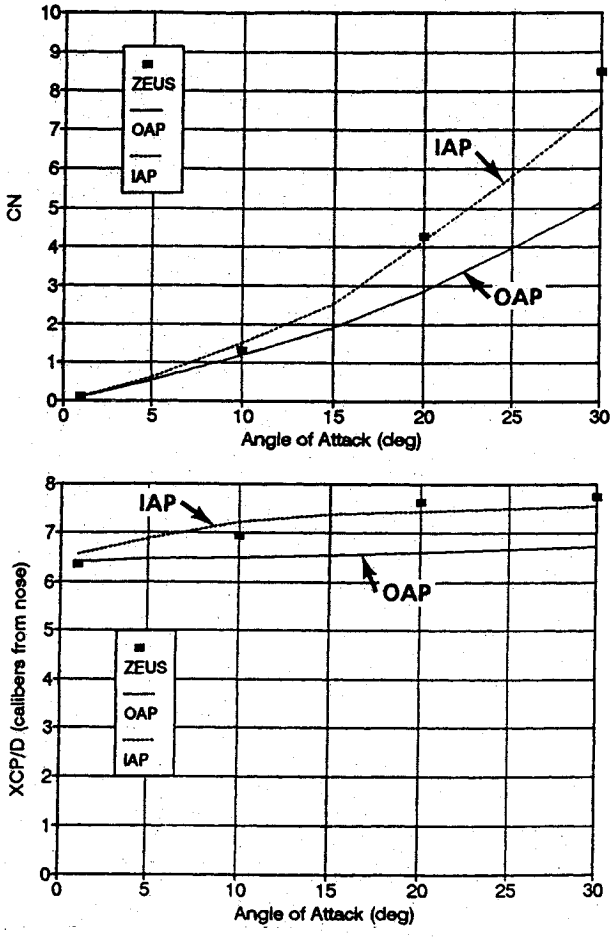

Fig. 11b Comparison of present normal force coefficient and center of pressure computations with the ZEUS code for a body-dorsal-tail configuration ($M_\infty = 10$).

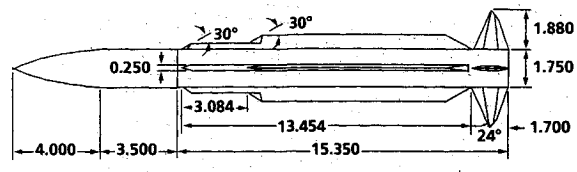

CONFIGURATION TESTED IN WIND TUNNEL (FROM REFERENCE 29 WHERE DIMENSIONS ARE IN INCHES)

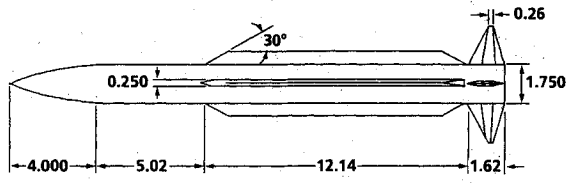

MODIFIED CONFIGURATION USED IN AEROPREDICTION COMPUTATIONS

PARAMETERSFOR BOTH MODELS

$(AR)_T = 4.0$	$b_t = 3.76$ in.	$\lambda_T = .16$	$(\Lambda_{LE})_T = 24°$	$A_T = 3.54$ in.^{2}
$(AR)_D = .12$	$b_D = 1.32$ in.	$\lambda_D = .77$	$(\Lambda_{LE})_D = 60°$	$A_D = 14.2$ in.^{2}

Fig. 12a Configuration used for comparison with missile DATCOM and experiment.

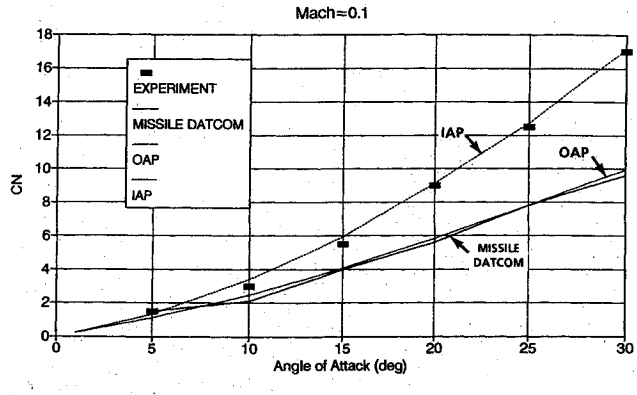

Fig. 12b Comparison of present normal force coefficient with that predicted by missile DATCOM and experiment.

Total Configuration Aerodynamics

Up to this point, only individual lift and center of pressure component aerodynamics have been considered. This section will deal only with total configuration aerodynamics to validate or find weaknesses in the new semiempirical technology. The configurations considered will include those within and outside of the databases from which the theory was developed. Those within the databases are the body-tail configurations common between the databases of Refs. 16 and 17. These configurations consist of the 12.33-caliber-long tangent-ogive-cylinder configuration (where the nose is 3 calibers long) mated to eight different wing planforms ($AR = 0.5$, $\lambda = 0$, 0.5, 1.0; $AR = 1.0$, $\lambda = 0.5$; $AR = 2.0$, $\lambda = 0$, 0.5, 1.0; $AR = 4.0$, $\lambda = 0.5$). Results of all of these cases are given in Ref. 21.

These eight configuration cases amount to 371 computational cases when investigated in increments of 5-deg angle of attack and at the Mach numbers of the database. When examined from a quantitative sense, the percent error for both C_N and X_{cp} of the OAP and IAP was computed for the 371 cases considered and averaged. The IAP reduced the error in normal force coefficient from an average of 11.7 for the OAP to 5.6%. Even more impressive was the consistency of the estimates. The worst case for the OAP was 51%, whereas for the IAP the worst case error was 20% with only a few cases with an error greater than 10%. For the center of pressure, the

average reduction in error was even more impressive. The average center of pressure error for the OAP was 2.9% of the body length (0.36 calibers), whereas the average error of the IAP was 1.2% of the body length (0.15 calibers). The maximum center of pressure error for the OAP was 11.2%, whereas for the IAP it was 5.3%. Although pitching moment comparisons are not shown, they should show comparable improvements. In general, the IAP has halved the normal force coefficient error when averaged over a large number of body-tail configurations and reduced the center of pressure error by over 60%.

Although these results are encouraging, it is expected that one should see improvements in normal force coefficient and center of pressure prediction accuracy when comparing against the database from which the new semiempirical theory was derived. The real test of the new theory will come in comparing normal force coefficient, center of pressure, and pitching moments on configurations outside the database.

Before examining other configurations outside the databases of Refs. 14–17, it is well to review the assumptions used in the semiempirical theory so as to check the robustness of the theory over a wide range of configurations and freestream conditions. The theory was derived for the following conditions: $0.6 \le M_\infty \le 4.6$, $0.25 \le AR \le 4.0$, $0 \le \lambda \le 1.0$, $r/s \le 0.5$, and body: 12.33-caliber ogive cylinder and 3.0-caliber tangent-ogive nose. Several of the cases chosen for validation of the new theory have parameters outside this range.

The first such case uses the same body as that of the database of Ref. 17, but with aspect ratio 2 tails and 0.1 dorsals (see Fig. 11a for the configuration). Mach numbers of 4.5 and 10 are considered in Ref. 21, and comparisons are made with

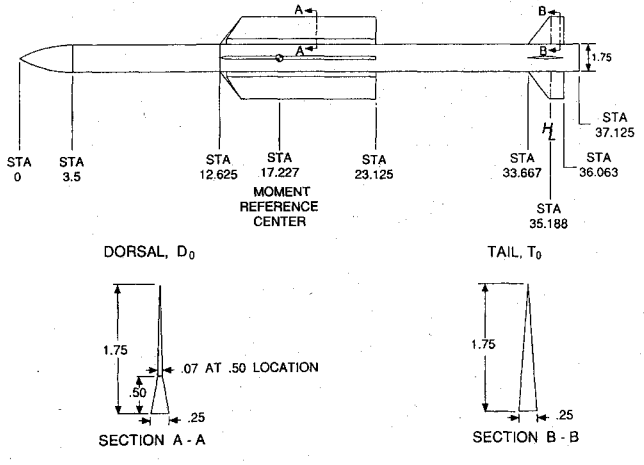

Fig. 13a Body-dorsal-tail configuration used for comparing missile 3, IAP, and OAP computations.

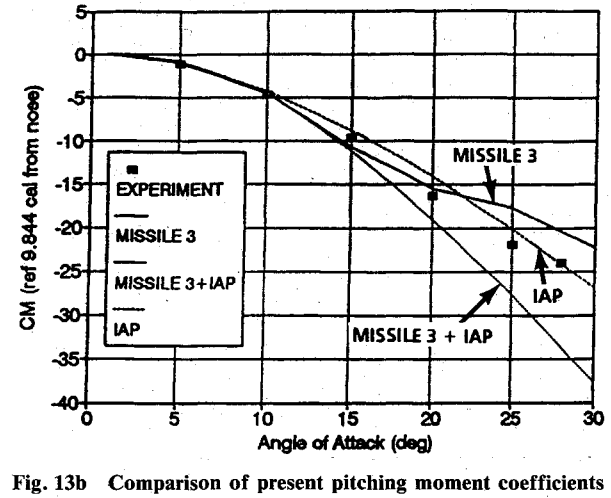

Fig. 13b Comparison of present pitching moment coefficients with missile 3 on a body-dorsal-tail configuration ($M_\infty = 4.6$).

the ZEUS code. Results of these comparisons in terms of normal force coefficient and center of pressure as a function of angle of attack are shown in Fig. 11b for the Mach 10 case. Center of pressure results show the IAP within 2% of the body length compared with the ZEUS computations at all angles of attack considered. On the other hand, the OAP center of pressure results differ by as much as 8% of the body length from the ZEUS code. In examining normal force coefficient comparisons, it is seen that at Mach 10 the IAP is within 13% of the ZEUS code, whereas the OAP results are off by as much as 40%. It is suspected that as aspect ratio gets small and as Mach number gets high, the viscous crossflow limit that was for wings ($\eta C_{d_c} = 0.95$) may approach that for bodies ($\eta C_{d_c} = 1.2$), which would account for the low value (11%) at $\alpha = 30$ and $M = 10$ of the IAP normal force coefficient compared with the ZEUS code. However, without wing-alone data at high Mach numbers, this is only a conjecture. Even with this error of up to 13% in normal force coefficient at $M = 10$, the results are acceptable for most engineering purposes.

The next configuration is taken from Ref. 29. It has dorsals that have an aspect ratio of 0.12 and tail surfaces that have an aspect ratio of 4.0. The aeroprediction code will not handle the configuration as shown at the top of Fig. 12a. Experience has shown that one needs to keep the lifting surface area, centroid of area, span, taper ratio, and aspect ratio the same. This means the tip and root chord of the dorsal and tail surfaces had to be adjusted with these constraints in mind. The new adjusted configuration is shown at the bottom of Fig. 12a. Hence, this configuration has all parameters outside the empirical database for use in the IAP, including Mach number, aspect ratio, body configuration, and r/s.

Only normal force coefficient results for the body-tail and body-dorsal-tail configurations at $M = 0.1$ were shown in Ref. 28. Results of the OAP, IAP, and Missile DATCOM[29] shown in Fig. 12b compared with experiment for the body-dorsal-tail configuration show that the IAP is clearly superior to both the OAP and Missile DATCOM. Normal force errors of the IAP are less than 5% at all conditions, whereas errors of the OAP and Missile DATCOM are as high as 40 and 50%, respectively. The fundamental reason for the IAP success is the nonlinear wing-alone normal force and interference factor methodology. At $\alpha = 30$ deg, the body dorsal and dorsal body contribute about ⅔ of the total configuration normal force.

The final configuration for validation of the new semiempirical methodology is shown in Fig. 13a. This configuration also differs substantially from the geometric characteristics from which the new methodology was derived. The body is 21.2 vs 12.33 calibers long with a 2-caliber von Kármán vs a 3-caliber tangent-ogive nose. The dorsals and tail surfaces have aspect ratios of 0.36 and 2.14, respectively, both at the outer edge of the database.

Wind-tunnel data exist for both the body-tail and body-dorsal-tail configuration (see Ref. 30) for Mach numbers of 2.3–4.6 and at several roll orientations. Comparisons were made at $\phi = 0$ deg roll and at Mach numbers of 2.3 and 4.6 for both the body-tail and body-dorsal-tail configurations in Ref. 21. Pitching moment coefficient results of the $M = 4.6$ case for the body-dorsal-tail configuration are shown in Fig. 13b. The IAP results are within the expected accuracy bounds on normal force, center of pressure, and pitching moment. Although OAP results are not shown for clarity, significant improvements in normal force for both body-tail and body-dorsal-tail configurations occur with less significant improvements in center of pressure. As noted in the comparisons, the IAP is superior to Missile 3[15] for most cases considered.

Summary

In summary, an improved body-alone nonlinear lift methodology and new semiempirical methods for wing-alone, wing-body, and body-wing interference lift have been developed. The new methods were based on the LT and SBT in the OAP but were modified to account for the appropriate physics

using wind-tunnel databases as a guide for angle-of-attack conditions. Simple engineering formulas were derived in many cases that can be used as general estimates of key aerodynamic terms. The new methodology is applicable to angles of attack of 30-deg and 0-deg roll angle.

Comparison of the new theory to the linear theory in the OAP showed significant improvements in static aerodynamic estimates. Comparison of the new theory to other engineering codes on a limited number of test cases showed it to be as good as or better than anything available. Even though the new semiempirical theory was developed based on a limited set of flight and geometric parameters, computations on configurations outside the database of parameters showed the new method to be robust.

Acknowledgments

Appreciation is expressed to Robin Staton and Dave Siegel, who manage and sponsor, respectively, the Surface-Launched Weapons Technology Block Program. Without funding provided by this program, this new work would not have been possible. Appreciation is also given to Frank Baltakis, who performed the ZEUS code computations for comparison with the present new approximate methods.

References

[1]Moore, F. G., "Computational Aerodynamics at NAVSWC: Past, Present, and Future," Naval Surface Warfare Center Dahlgren Division, NAVSWC TR 90-569, Dahlgren, VA, Oct. 1990.

[2]Devan, L., "Aerodynamics of Tactical Weapons to Mach Number 8 and Angle of Attack 180°: Part I, Theory and Application," Naval Surface Warfare Center Dahlgren Division, NSWC TR 80-346, Dahlgren, VA, Oct. 1980.

[3]Devan, L., and Mason, L., "Aerodynamics of Tactical Weapons to Mach Number 8 and Angle of Attack 180°: Part II, Computer Program and Users Guide," Naval Surface Warfare Center Dahlgren Division, NSWC TR 81-358, Dahlgren, VA, Sept. 1981.

[4]Devan, L., Mason, L., and Moore, F. G., "Aerodynamics of Tactical Weapons to Mach Number 8 and Angle of Attack 180°," AIAA Paper 82-0250, Jan. 1982.

[5]Moore, F. G., "Body Alone Aerodynamics of Guided and Unguided Projectiles at Subsonic, Transonic and Supersonic Mach Numbers," Naval Surface Warfare Center Dahlgren Division, NWL TR-2796, Dahlgren, VA, Nov. 1972.

[6]Van Dyke, M. D., "First- and Second-Order Theory of Supersonic Flow Past Bodies of Revolution," *Journal of Aeronautical Sciences,* Vol. 18, No. 3, 1951, pp. 161–179.

[7]DeJarnette, F. R., Ford, C. P., and Young, D. E., "A New Method for Calculating Surface Pressures on Bodies at an Angle of Attack in Supersonic Flow," AIAA Paper 79-1552, July 1974.

[8]Moore, F. G., Armistead, M., Rowles, S. H., and DeJarnette, F. R., "Second-Order Shock-Expansion Theory Extended to Include Real Gas Effects," Naval Surface Warfare Center Dahlgren Division, NAVSWC TR 90-683, Dahlgren, VA, Feb. 1992.

[9]Allen, J. H., and Perkins, E. W., "Characteristics of Flow over Inclined Bodies of Revolution," NACA RM A 50L07, March 1951.

[10]Chadwick, W. R., "The Application of Non-Planer Lifting Surface Theory to the Calculation of External Store Loads," *AIAA Journal,* Vol. 11, No. 3, 1974, pp. 181–188.

[11]Martin, J. C., and Jefferys, I., "Span Load Distribution Resulting from Angle of Attack, Rolling, and Pitching for Tapered Sweptback Wings with Streamwise Tips," NACA TN 2643, July 1952.

[12]Douglas Aircraft Company, Inc., "USAF Stability and Control DATCOM," Flight Control Division, Air Force Flight Dynamics Lab., AF/56780/7000, Wright Patterson AFB, OH, 1974.

[13]Aiello, G. F., "Aerodynamic Methodology (Bodies with Tails at Arbitrary Roll Angles, Transonic and Supersonic)," Martin Marietta Corp., OR 14, 145, Orlando, FL, April 1976.

[14]Nielsen, J. N., Hemsch, M. J., and Smith, C. A., "A Preliminary Method for Calculating the Aerodynamic Characteristics of Cruciform Missiles to High Angles of Attack Including Effects of Roll Angle and Control Deflections," Office of Naval Research, ONR Rept. CR 215-226-4F, Arlington, VA, Nov. 1977.

[15]Lesieutre, D. J., Mendenhall, M. R., Nazario, S. M., and Hemsch, M. J., "Prediction of the Aeroprediction Characteristics of Cruciform Missiles Including Effects of Roll Angle and Control Deflection," Nielsen Engineering and Research, TR 360, Mountain View, CA, Aug. 1986.

[16]Stallings, R. L., Jr., and Lamb, M., "Wing-Alone Aerodynamic Characteristics for High Angles of Attack at Supersonic Speeds," NASA TP 1889, July 1981.

[17]NASA Langley Research Center Tri-Service Missile Data Base, transmitted from NASA/LRC Jerry M. Allen to NAVSWC on 5 Nov. 1991 (formal documentation in process).

[18]Lucero, E. F., "Empirical Curves for Predicting Supersonic Aerodynamics of Very Low Aspect Ratio Lifting Surfaces," AIAA Paper 84-0575, Jan. 1984.

[19]Hoerner, S. F., "Characteristics of Small Aspect Ratio Wings," *Fluid Dynamics Lift,* published by Liselotte Hoerner, Box 342, Brick Town, NJ, 08723, 1975, Chap. XVII.

[20]Polhamus, E. C., "Predictions of Vortex-Lift Characteristics by a Leading Edge Suction Analogy," AIAA Paper 69-1133, Oct. 1969.

[21]Moore, F. G., Hymer, T., and Devan, L., "New Methods for Predicting Nonlinear Lift, Center of Pressure, and Pitching Moment on Missile Configurations," Naval Surface Warfare Center Dahlgren Division, NSWCDD/TR-92/217, Dahlgren, VA, July 1992.

[22]Moore, F. G., "Aerodynamics of Guided and Unguided Weapons: Part I—Theory and Application," Naval Surface Warfare Center Dahlgren Division, NWL TR-3018, Dahlgren, VA, Dec. 1973.

[23]Evvard, J. C., "Use of Source Distributions for Evaluating Theoretical Aerodynamics of Thin Finite Wings at Supersonic Speeds," NACA Rept. 951, 1950.

[24]Wardlaw, A. B., Jr., Baltakis, F. P., Martin, F. M., and Priolo, F. J., "A Godunov Method for Supersonic Tactical Missiles," *Journal of Spacecraft and Rockets,* Vol. 24, No. 1, 1987, pp. 40–47.

[25]Hoerner, S. F., *Fluid-Dynamic Drag,* Hoerner Fluid Dynamics, P.O. Box 342, Brick Town, NJ, 08723, 1965.

[26]Jorgensen, L. H., "Prediction of Static Aerodynamic Characteristics for Slender Bodies Alone and with Lifting Surfaces to Very High Angles of Attack," NASA TR R-474, Sept. 1977.

[27]Pitts, W. C., Nielsen, J. N., and Kaattari, G. E., "Lift and Center of Pressure of Wing-Body-Tail Combinations at Subsonic, Transonic, and Supersonic Speeds," NACA TR 1307, 1957.

[28]Howard, R. M., and Dunn, A., "Missile Loads at High Angles of Attack," *Journal of Spacecraft and Rockets,* Vol. 28, No. 1, 1991, p. 124.

[29]Vukelich, S. R., Stoy, S. L., Burns, K. A., Castillo, J. A., and Moore, M. E., "Missile DATCOM Vol. I—Final Report," Air Force Wright Aeronautical Lab., AFWALTR-86-3091, Wright Patterson AFB, OH, Dec. 1988.

[30]Bibel, J. E., and Hardy, S. R., "Wind Tunnel Test Data of the High Performance Point Defense Missile (HPPDM) Obtained in the NASA Langley Unitary Plan Wind Tunnel," Naval Surface Warfare Center, Dahlgren Division, NAVSWC TR 90-475, Dahlgren, VA (to be published).

Jerry M. Allen
Associate Editor